

Optimal sizing of 1D vibrating columns accounting for axial compression and self-weight

Federico Ferrari^{a,*}

^a*Department of Civil and Mechanical Engineering, Technical University of Denmark, Koppels Allé, 2800 Lyngby, Denmark*

Abstract

We investigate the effect of axial compression on the optimal design of columns, for the maximization of the fundamental vibration frequency. The compression may be due to a force at the columns' tip or to a load distributed along its axis, which may act either independently or simultaneously. We discuss the influence of these contributions on the optimality conditions, and show how the optimal beam design, and the corresponding frequency gain drastically change with the level of compression. We also discuss the indirect effect of frequency optimization on the critical load factors for the tip (λ_P) and distributed (λ_Q) loads. Finally, we provide some quantitative results for the optimal design problem parametrized by the triple (λ_P , λ_Q , Ω^2) of buckling and dynamic eigenvalues.

Keywords: Optimal design, Eigenvalue optimization, Vibration, Buckling

1. Introduction

Sizing of beams is a classical topic within optimal structural design, and has been one of the driving applications in the early developments of the field[5, 51, 22]. Despite the simplicity of beam models, closed-form solutions to their optimal design are achievable only in a few cases, involving compliance, volume, or displacement objective or constraints, and linear elastic beams[21, 30, 49, 44], plastic design[51, 15, 50], or design against buckling of uniformly compressed, statically determined columns[34, 47]. In more advanced instances, such as optimization of vibration frequencies, or buckling loads for general boundary conditions and loads, the beams' optimal size can only be computed by numerical methods.

Nevertheless, important insights about the qualitative behavior of the solution can still be obtained through local asymptotic analysis[26], and bounds on the optimal frequencies or buckling loads can be given by isoperimetric inequalities[43, 55]. For instance, Niordson[39] studied the optimal design of a simply supported beam for maximum fundamental frequency of vibration, showing an optimal improvement of 6.6%. The analysis was extended to the cantilever beam by Karihaloo and Niordson[33], giving a much higher frequency improvement: 425-678%, depending on the relationship between stiffness and inertia, and then to the optimization of higher frequencies by Olhoff[40]. These studies highlighted some delicate matters, which have been the focus of many later works, both dealing with vibration and buckling optimization.

First, at points where the beam's internal actions vanish, the optimal beam size will also go to zero, causing a singularity in one of the generalized displacement or strain components[41]. In particular, at locations where only the bending moment vanishes a hinge-like point appears (Type I singularity[21]), whereas at locations where both the bending moment and shear force vanish a complete separation of the beam (Type II singularity[40]) can occur. This may compromise the well-position of the Sturm-Liouville operator underlying the optimal design problem, [9, 6, 7], and several works have focused on finding the correct setting, and admissible class of optimal size distributions to avoid this[37, 14, 19].

Another delicate point concerns the very existence of non-trivial optimal solutions, depending on the relationship between stiffness and mass, the introduction of design-independent inertia terms, and the particular choice of boundary conditions[46]. These matters have been the focus of many mathematical studies, such as those by Brach[11, 12], Holmâker [27], and Vepa[57].

The literature on optimal beam design against buckling is equally vast [13]. Limiting the discussion to recent times, Keller[34] started it off by giving a closed-form solution for the optimal design of a simply supported column

*Corresponding author

Email address: `feferr@dtu.dk` (Federico Ferrari)

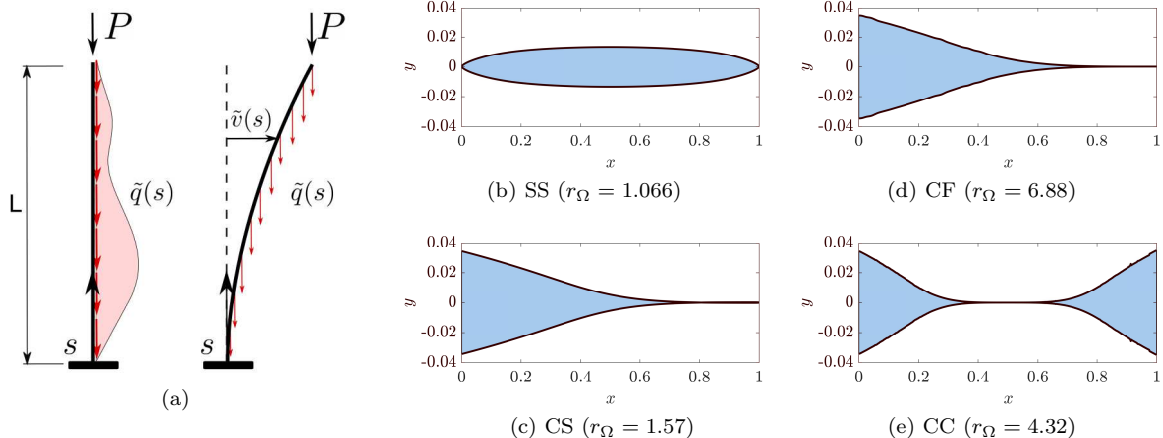


Figure 1: (a) Sketch of a column loaded by the tip force P and distributed axial load $\tilde{q}(s)$, considering the cantilever configuration. (b) Optimal size distribution, maximizing the fundamental frequency of vibration Ω_1 , for the four cases of boundary conditions: simply supported (SS), cantilever (CF), clamped-pinned (CP), and fully clamped (CC). For each case, r_Ω is the maximum relative frequency gain, given by [39, 40]

with maximum buckling load, under a uniform tip compression. Then, Tadjbakhsh and Keller [55] extended to other boundary conditions, including the clamped beam, and this latter case was then reassessed by Olhoff and Rasmussen [42], accounting for the bimodal character of the optimal solution. The design of a heavy column, where the compression varies along the beam's axis according to self-weight, was addressed by Keller and Niordson [35], using a combination of asymptotic and numerical methods. In this case, the same technical caveats encountered for frequency optimization are raised, as discussed by Cox and McCarthy [16, 38], or Barnes [10, 8], who introduced minimum requirements on the optimal beam size to ensure well position of the problem. From a more practical stance, the regularization of the problem by introduction of a minimum size had already been proposed by Adali [1].

Buckling design under the combined effect of self-weight and a tip, design-independent compression, was studied by Atanackovic, [2], also considering the bimodal optimization of the clamped column [3, 4]. Other recent works on the topic are from Sadiku [52, 53], Seyranian and Privalova [54], and Egorov [17, 18].

In the author's knowledge, no research work has yet systematically addressed the interplay between buckling and frequency optimization, while considering self-weight. The work by Rammerstorffer [47] is the only one we are aware of discussing the influence of a pre-stress on the beam frequency optimization problem. However, the analysis was limited to uniform pre-stress, simply supported configuration, and a linear control, since the design variable was the Young's modulus.

As the optimal size of frequency optimized beams shows large variations, and the tendency to vanish at some locations, a question about the beams' stability naturally arises. The designs in Figure 1 suggest that the buckling strength of beams optimized purely for vibrations may be severely compromised, to the extent that even self-weight may trigger instability.

Here we aim at providing a broad analysis of the influence of compression on the optimization outcomes. We address the classical problem of maximizing the fundamental frequency of vibration, introducing both constant (size-independent) and variable (size-dependent) compression sources. First, we discuss how these enter the optimally conditions of the problem, also considering the particular case of self-weight. Then, we provide numerical results considering the two compression sources acting either separately or simultaneously. We will show that both substantially change the optimized design, and, generally, also the frequency improvement which can be obtained. Depending on the beam's boundary conditions, and for a compression which is close to the critical one, the natural frequency increases between 7 to 14.2 times, when the applied compression is uniform, and up to 15 times when it is size-dependent. These improvements are much higher than those achieved when optimizing an unloaded beam [39, 33], making frequency optimization even more appealing for higher compressed beams [47].

We also discuss the indirect effect that the optimal design process has on the buckling capacity of the beam. Again, this heavily depends on the amount of compression considered in the optimization, and it is not obvious that the optimized design is stronger than the uniform one as soon as we account for compression in the optimization process.

Finally, we point out that here we consider the technical Bernoulli beam model, following the majority of the research works in the field. Relatively few works have dealt with the Timoshenko beam [29, 32, 36], or with geometrically nonlinear models [20, 45], or again with non-conservative loads [23, 48].

2. Governing equations and statement of the optimization problem

We consider the initially slender, straight, non-uniform column depicted in Figure 1(a), whose axis occupies the interval $[0, L] \subset \mathbb{R}$. The column is subjected to the tip force of magnitude P , and to the distributed axial load with intensity $\tilde{q}(s)$, $s \in (0, L)$, both inducing compression.

Assuming the moderately nonlinear kinematic Bernoulli theory, the Lagrangian density associated with the beam's small amplitude transversal vibrations is

$$\ell [s, \tilde{v}(s, t)] = \frac{1}{2} \left[\rho A \tilde{v}_t^2 + \left(P + \int_s^L \tilde{q}(\zeta) \, d\zeta \right) \tilde{v}_s^2 - EJ \tilde{v}_{ss}^2 \right] \quad (1)$$

where s and t are the space and time coordinates, $\tilde{v}(s, t)$ is the lateral deflection, $A = A(s)$, $\rho = \rho(s)$, $J = J(s)$ and $E = E(s)$ are the beam area, density, modulus of inertia and Young's modulus, respectively. In Equation (1), and later on, subscript lowercase letters will denote differentiation with respect to the corresponding variable.

Taking one characteristic dimension of the cross section as variable over the beam length, according to the function $\tilde{y}(s) \in \mathcal{Y} := \{y \in C^0(0, L) \mid \tilde{y}_{\min} \leq \tilde{y}(s) \leq \tilde{y}_{\max}\}$ [37, 10], the area becomes $A(s) = y_0 \tilde{y}(s)$, where y_0 is a constant length [28, 25]. The modulus of inertia can be expressed as

$$J(s, p) = c_1 A(s)^p = \alpha y_0^{2(2-p)} [y_0 \tilde{y}(s)]^p = \alpha y_0^{(4-p)} \tilde{y}^p(s) \quad (2)$$

where $c_1 = \alpha y_0^{2(2-p)}$, $\alpha \in \mathbb{R}$, and $p \in \mathbb{N}_+$ (usually, $p = \{1, 2, 3\}$). Choosing the y_0 and p , (2) can be particularized to the case of some commonly used cross sections shapes [44].

Introducing the non-dimensional variables $x = s/L$, $\tau = t/T$, $v(x, \tau) = \tilde{v}(s, t)/L$, $y(x) = y_0 L \tilde{y}(s)/V$, and $q(x) = L \tilde{q}(s)/Q$, where V is the beam's volume and $Q = \int_0^L \tilde{q}(s) \, ds$ the magnitude of the distributed load, the substitution of (2) in (1) gives

$$\ell [x, v(x, \tau)] = \frac{1}{2} \left[\varpi y v_\tau^2 + \left(\lambda_P + \lambda_Q \int_x^1 q(\zeta) \, d\zeta \right) v_x^2 - y^p v_{xx}^2 \right] \quad (3)$$

where we have introduced the non-dimensional parameters

$$\lambda_P = \frac{P}{V\beta}, \quad \lambda_Q = \frac{Q}{V\beta}, \quad \varpi = \frac{\rho L}{T^2\beta} \quad (4)$$

and $\beta = E\alpha V^{p-1} y_0^{4-2p}/L^{p+2}$.

For $\lambda_P < \lambda_P^{(\text{Cr})}$ and $\lambda_Q < \lambda_Q^{(\text{Cr})}$, where $\lambda_P^{(\text{Cr})}$ and $\lambda_Q^{(\text{Cr})}$ are the critical multipliers for the tip force and distributed load, respectively, the beam will undergo small amplitude harmonic oscillations. Therefore, we assume $v(x, \tau) = v(x)e^{-i\omega\tau}$ and $v_\tau^2 = -\omega^2 v^2(x)$ ($\omega > 0$), and imposing stationarity of (3) with respect to $\delta v \in \mathcal{V} := H_0^2(0, 1)$ gives the elasto-dynamic linear field equation governing the beam's motion

$$(y^p v_{xx})_{xx} + \left(\lambda_P + \lambda_Q \int_x^1 q(\zeta) \, d\zeta \right) v_{xx} - \lambda_Q q(x) v_x - \Omega^2 y v = 0 \quad x \in (0, 1) \quad (5)$$

where $\Omega^2 := \varpi \omega^2$ is the dynamic eigenvalue, proportional to the square of the angular frequency ω . The boundary terms arising from the integration by parts of (3) can be collected in the linear operator

$$B[v, \delta v] := \left[(y^p v_{xx})_x + \left(\lambda_P + \lambda_Q \int_x^1 q(\zeta) \, d\zeta \right) v_x \right] \delta v - y^p v_{xx} \delta v_x \Big|_{x=\{0,1\}} \quad (6)$$

corresponding to one of the following pairs of boundary conditions at $x = \{0, 1\}$

$$\begin{aligned} \text{either } v = 0 \quad \text{or } (y^p v_{xx})_x + \left(\lambda_P + \lambda_Q \int_x^1 q(\zeta) \, d\zeta \right) v_x = 0 \\ \text{either } v_x = 0 \quad \text{or } y^p v_{xx} = 0 \end{aligned} \quad (7)$$

When the distributed axial load is proportional to self-weight, we have $\tilde{q}(s) = \rho g A(s) = \rho g y_0 \tilde{y}(s)$ and (5) and (6) hold with $q(\zeta) = y(\zeta)$ and $\lambda_Q = \rho g \beta^{-1}$.

2.1. Optimization problem and solution strategy

We aim at finding the optimal size distribution $y_* \in \mathcal{Y}$ maximizing the beam's fundamental frequency $\Omega_1 = \Omega_1(\lambda_P, \lambda_Q)$, for a prescribed total volume fraction V and compression level, given by the pair (λ_P, λ_Q) . This can be stated as

$$\begin{aligned} \max_{y \in \mathcal{Y}} \Omega_1^2(\lambda_P, \lambda_Q) &:= \left\{ \min_{v \in \mathcal{V}-0} \frac{\langle y^p v_{xx}, v_{xx} \rangle_{[0,1]} - \langle (\lambda_P + \lambda_Q I[x, y]) v_x, v_x \rangle_{[0,1]} }{\langle yv, v \rangle_{[0,1]}} \right\} \\ &\text{s.t. } \langle y, 1 \rangle_{[0,1]} - 1 \leq 0 \end{aligned} \quad (8)$$

where we have introduced the shorthand notation $\langle u, v \rangle_{[a,b]} = \int_a^b uv \, dx$, and set $I[x, y] = \langle q(\xi, y(\xi)), 1 \rangle_{[x,1]}$. In this latter term we account for a general dependence on both x and y , allowing for the case of self-weight.

The objective of (8) is the squared frequency, reduced by both the tip and axially distributed compression, and expressed through the Rayleigh quotient[59]. This can be related to the one of the unloaded beam $\bar{\Omega}_1^2$ by

$$\Omega_1^2(\lambda_P, \lambda_Q) = \bar{\Omega}_1^2 - \langle (\lambda_P + \lambda_Q I[x, y]) v_x, v_x \rangle_{[0,1]} \quad (9)$$

where, without loss of generality, we assumed $\langle yv, v \rangle_{[0,1]} = 1$. Equation (9) expresses the well-known inverse proportionality between the squared natural frequency and axial compression [58], and we remark that $\Omega_1^2 = 0$ when either $\lambda_P = \lambda_P^{(\text{Cr})}$ or $\lambda_Q = \lambda_Q^{(\text{Cr})}$.

Taking the variation of the Lagrangian associated with (8), with respect to $\delta y \in \mathcal{Y}$, we obtain the adjoint equation

$$py^{p-1}v_{xx}^2 - \lambda_Q I_y[x, y]v_x^2 - \Omega_1^2 v^2 - \mu = 0 \quad (10)$$

where $I_y[x, y] = \delta I[x, \delta y]$ and $\mu \in \mathbb{R}_+$ is the Lagrange multiplier associated with the volume constraint. Assuming that such constraint is active at the optimum [5], we have

$$\mu_* = (p-1)\bar{\Omega}_1^2 + \langle [\lambda_P + \lambda_Q (I[x, y] - yI_y[x, y])] v_x, v_x \rangle_{[0,1]} \quad (11)$$

The optimal beam size distribution is then found by solving (10) with respect to y

$$y_*(x) = \left[\frac{\mu + \lambda_Q I_y[x, y]v_x^2 + \Omega_1^2 v^2}{pv_{xx}} \right]^{1-p} \quad (12)$$

and once this is known, the optimal displacement v_* is computed from (5), paired with the appropriate set of boundary conditions from (7), and the eigenvalue Ω_{1*}^2 is given by the condition $\langle y, 1 \rangle_{[0,1]} = 1$.

The set of nonlinear field equations governing the state, adjoint and optimal size is summarized here

$$\begin{aligned} 0 &= (y^p v_{xx})_{xx} + \gamma_1 v_{xx} - \gamma_0 v_x - \bar{\Omega}_1^2 yv \\ 0 &= py^{p-1}v_{xx}^2 - \gamma_2 v_x^2 - \left(\bar{\Omega}_1^2 - \langle \gamma_1 v_x, v_x \rangle_{[0,1]} \right) v^2 - (p-1)\bar{\Omega}_1^2 - \langle (\gamma_1 - y\gamma_2) v_x, v_x \rangle_{[0,1]} \\ y &= \left[\frac{\gamma_2 v_x^2 + \left(\bar{\Omega}_1^2 - \langle \gamma_1 v_x, v_x \rangle_{[0,1]} \right) v^2 + (p-1)\bar{\Omega}_1^2 + \langle (\gamma_1 - y\gamma_2) v_x, v_x \rangle_{[0,1]}}{pv_{xx}} \right]^{1-p} \end{aligned} \quad (13)$$

where we have set $\gamma_0 := \lambda_Q q(x)$, $\gamma_1 := \lambda_P + \lambda_Q I[x, y]$, and $\gamma_2 := \lambda_Q I_y[x, y]$.

Equation (13) is a system of non-linear, coupled, integro-differential equations expressing the optimality conditions for the optimization problem of (8). We notice that the design variable y enters non-linearly in both the state and adjoint equations, whereas the state variable v appears only linearly in the state equation, as the coefficients γ_i do not depend on it. Also, we remark that in (13) we have written everything in terms of the eigenvalue of the unloaded beam $\bar{\Omega}_1^2$, and explicitly substituted for the Lagrange multiplier expression (11), to fully show the influence of each term, in the most general case. However, we will see in the following example that (13) can be considerably simplified, when tackling specific cases.

3. Numerical results

We consider a slender beam with aspect ratio $L/y_0 = 12$, where $y_0 = 0.5$ is the constant cross section dimension, and also the upper bound \tilde{y}_{\max} for the size distribution. The maximum allowed volume is $V = 0.25y_0L$, and the Young modulus and density are $E = 2.5 \cdot 10^7$ MPa and $\rho = 2.4 \text{ kg/m}^3$. We assume similar cross sections[44], setting $p = 2$ and $\alpha = 1/12$ in (2). Four cases of boundary conditions, also called beam configurations in the following, are considered: cantilever (CF), simply supported (SS), doubly clamped (CC) and clamped-pinned (CP).

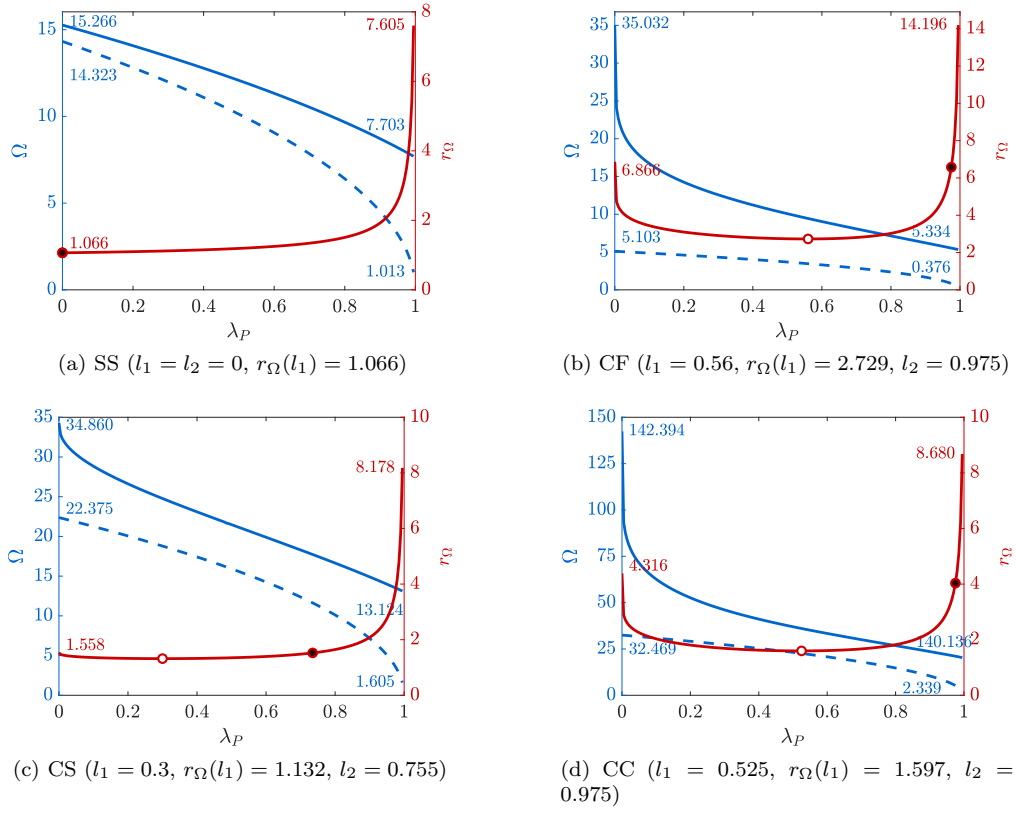


Figure 2: Relationship between the normalized tip compression λ_P and the frequency of the uniform (Ω_0 , blue dashed curve), and optimized beams (Ω_* , blue continuous curve). The frequency gains obtained by solving (8) for each λ_P , say r_Ω , are plotted as a red continuous curve. For the CF, CS, and CC beams r_Ω is non-monotonic and attains the minimum value at $\lambda_P = l_1$ (white dot), whereas $\lambda_P = l_2$ (black dot) corresponds to the condition $r_\Omega(l_2) = r_\Omega(0)$

The solution strategy for (8) is based on iterating between the state and adjoint equations (13), until both conditions $\|y(k) - y(k-1)\|_\infty \leq 10^{-3}$ and $|\Omega(k) - \Omega(k-1)| \leq 10^{-4}$ are fulfilled. This is carried out repeatedly, starting by setting the lower bound $\tilde{y}_{\min} = 10^{-3}$, then reducing it until $\tilde{y}_{\min} = 10^{-10}$. In each of these steps, we use the final size distribution from the previous one as initial guess. We will take that a given design shows a Type I, or Type II singularity[40] if its final size distribution y_* hits \tilde{y}_{\min} at an isolated point, or at multiple adjacent points, respectively. The state variable v_h is discretized by C^1 elements [31], ensuring nodal continuity of both v and v_x , whereas the design variable y_h is only continuous at nodes.

In the following, the tip compression is scaled by $\lambda_P/\lambda_{P(0)}^{\text{Cr}} \in [0, 1)$, where $\lambda_{P(0)}^{\text{Cr}} = L_c^{-2}\pi^2 EJ_0$ is the critical load of the uniform beam, and L_c is the characteristic length depending on the boundary conditions [56]. Likewise, the distributed axial load is scaled by $\lambda_Q/\lambda_{Q(0)}^{\text{Cr}} \in [0, 1)$, where $\lambda_{Q(0)}^{\text{Cr}}$ is the critical load corresponding to a constant load distribution. To ease the notation, we will denote these multipliers by the symbols λ_P and λ_Q . As we focus on the fundamental vibration frequency, we drop the subscript “1”, and we denote the frequencies of the uniform and optimized size distributions by Ω_0 and Ω_* , respectively. Also, we will call “reduced frequencies” those reduced by the axial compression through (9).

3.1. Influence of the tip force alone ($\lambda_P \geq 0$, $\lambda_Q = 0$)

In this case $\gamma_0 = \gamma_2 = 0$, $\gamma_1 = \lambda_P$, and the state and adjoint equations in (13) simplify to

$$\begin{aligned} 0 &= (y^p v_{xx})_{xx} + \lambda_P v_{xx} - \bar{\Omega}^2 yv \\ 0 &= py^{p-1} v_{xx}^2 - \left(\bar{\Omega}^2 - \lambda_P \langle v_x, v_x \rangle_{[0,1]} \right) v^2 - (p-1)\bar{\Omega}^2 - \lambda_P \langle v_x, v_x \rangle_{[0,1]} \end{aligned} \quad (14)$$

and the design-independent compression influences the solution of (8) through the state equation and the Lagrange multiplier μ .

The compression, which is constant during the optimization, is applied in the range $\lambda_P \in [0, 0.995]$, with $\Delta\lambda_P = 1/200$. We refer to the smallest level of non-zero compression ($\lambda_P = 0.005$) as $\lambda_P \approx 0$, and to the last multiplier as $\lambda_P \approx 1$. The BLF of the beam, say λ_P^{Cr} , will be indirectly modified during the optimization, and we must check that

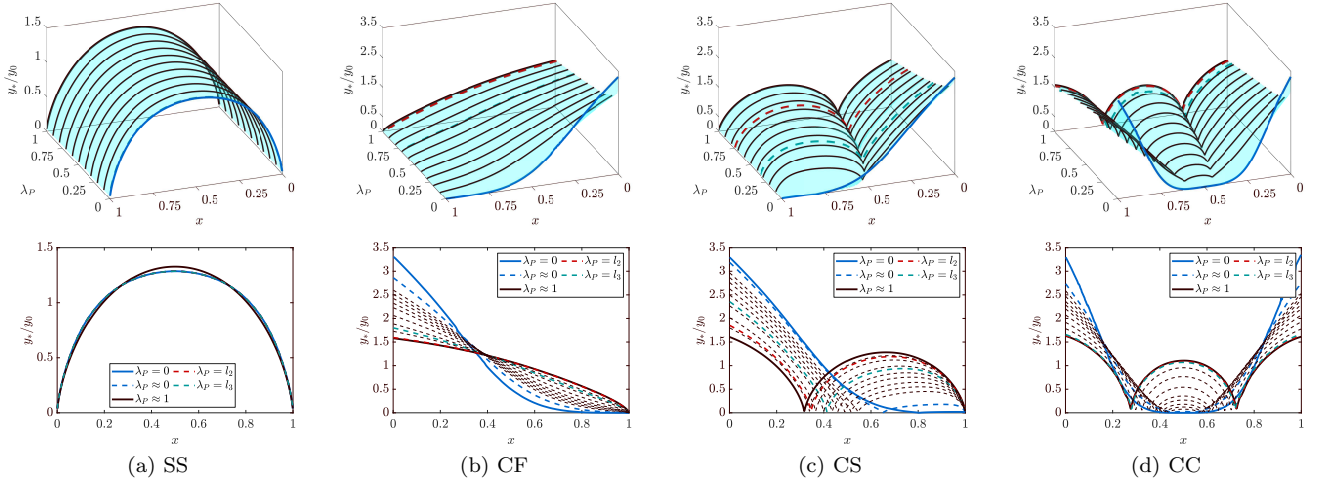


Figure 3: Optimized size distribution $y_*(x)$, relative to the initial one y_0 , for each beam configuration. On the 3D views, we highlight the designs corresponding to the tip compression values: $\lambda_P = 0$ (blue), $\lambda_P \approx 1$ (black), and $\lambda_P = l_2$ (red). This latter corresponds to $r_\Omega(l_2) = r_\Omega(0)$, and the frequency gain equals that of the optimal unloaded beam. The same designs are highlighted on the 2D views, where we also mark the one corresponding to the slightest applied compression $\lambda_P \approx 0$ (blue dashed curve)

$\lambda_P \leq \lambda_P^{\text{Cr}}$ at each step (see Subsection 3.4); otherwise the beam will undergo divergence, voiding the assumption of harmonic motion.

Figure 2 shows the influence of the compression level on the frequency of the uniform beam (Ω_0 , blue dashed line), and of the optimized one (Ω_* , blue continuous line). While the first follows the well-known (nearly) inverse proportionality between Ω_0^2 and λ_P [58], the frequency attained in the optimization decreases less than proportionally with the compression level. The relative frequency gain corresponding to each compression level is given by the ratio $r_\Omega := \Omega_*/\Omega_0$ (see red line in Figure 2). For $\lambda_P = 0$ (optimization of the unloaded beam), r_Ω attains values very close to the theoretical bounds recalled in Figure 1 (b). We clearly have $r_\Omega \rightarrow \infty$ as $\lambda_P \rightarrow 1$; however, we recall that we bound λ_P to be close but slightly below one. The largest absolute r_Ω is reached by the CF configuration, which for $\lambda_P \approx 1$ shows a frequency gain of over 14 times, whereas the SS configuration is the one showing the largest relative improvement between $r_\Omega(0)$ (unloaded beam) and $r_\Omega(\approx 1)$ (highly compressed beam).

For all the configurations but the SS, the relationship between λ_P and r_Ω is non-monotonic. For the CF, CS and CC beams, as soon as $\lambda_P > 0$ the frequency attained by the optimized beam (Ω_*) decreases much more rapidly than the frequency of the uniform one, and r_Ω drops. After reaching a minimum at $\lambda_P = l_1$ (white dot in Figure 2), the frequency gain r_Ω equals the one for the unloaded beam at $\lambda_P = l_2$ (black dot in Figure 2), then increases further as $\lambda_P \rightarrow 1$.

This non-monotonic behaviour can be explained by looking at how the optimized size distribution $y_*(x)$ changes with the increase of the compression (Figure 3). For the SS beam, the optimized size shows minor changes and only gets thicker near the beam center, and more flat near the pinned ends, as λ_P increases. For all the other beam configurations, the optimized size shows an abrupt change as soon as $\lambda_P > 0$, and immediately adapts to sustain the design-independent tip load. The size distribution is prevented from vanishing according to a Type II singularity, whereas we still have points resembling a Type I singularity, where the bending moment vanishes (see Appendix A). For the CS and CC configurations, these points appear within the beam domain as soon as $\lambda_P > 0$ and, for $\lambda_P \approx 1$, they are at $x \approx 1/3$ and $x \approx 1/6$, respectively[21]. However, we stress that these points do not strictly correspond to singularities, since we always have $y_* > y_{\min}$, as soon as $\lambda_P > 0$.

The optimized design shown as a red dashed line in Figure 3 corresponds to the compression level $\lambda_P = l_2$, where we match the frequency gain of the unloaded beam. We also plot, as green dashed line, the one corresponding to $\lambda_P = l_3$; this is the first designs meeting the same buckling strength of the uniform beam, as will be further discussed in Subsection 3.4.

The above discussion shows that for the CF, CS, and CC beams the magnitude of λ_P has a huge effect on the frequency optimization. Even the slightest design-independent compression prevents the optimal beam size from vanishing according to a Type II singularity, and this drastically lowers the frequency gain. Then, as the compression level increases, the reduction in the initial frequency is so severe that the frequency gain becomes even higher than the one reached when optimizing the unloaded beam. For the SS beam, the frequency gain is always higher for the compressed beam, compared to the unloaded one.

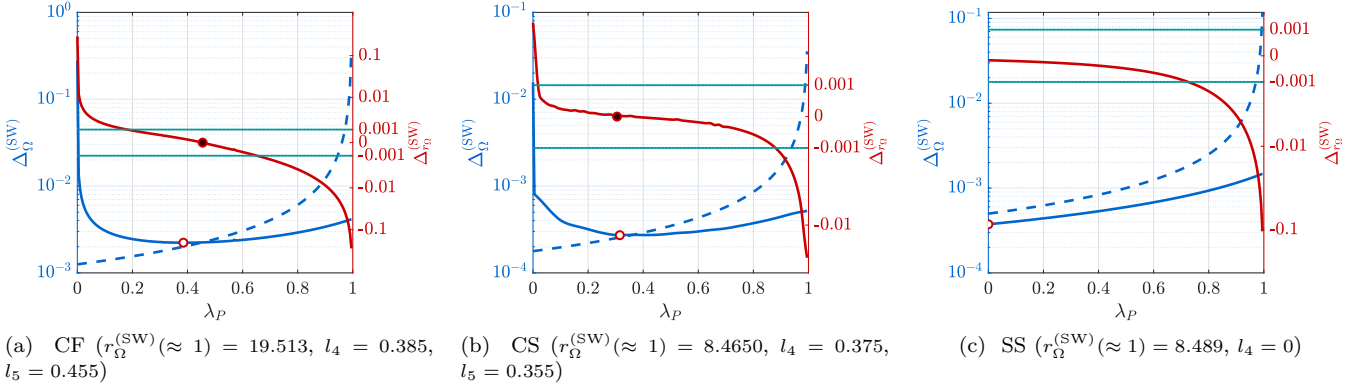


Figure 4: Relationship between the normalized tip compression λ_P and the relative reduction in the frequency due to the self-weight, for the uniform (blue dashed curve), and optimized (blue continuous curve) beams. The red curve shows the relative reduction of the frequency gains $\Delta_{r_{\Omega}}^{(SW)}$. All curves are scaled according to the log-abs transform. The white dot marks the point $\lambda_P = l_4$, where we have the minimum of $\Delta_{\Omega}^{(SW)}$, and the black dot marks the point $\lambda_P = l_5$, where $\Delta_{r_{\Omega}}^{(SW)} = 0$; thus the self-weight has no influence on the frequency gain. The horizontal dotted lines bound the region where $|\Delta_{r_{\Omega}}^{(SW)}| \leq 10^{-3}$. For the CC configuration the trend is basically the same as for the CS, and we refer to Table 1 for numerical values

3.2. Influence of the self-weight ($\lambda_P \geq 0$, $q(x) = y(x)$, $\lambda_Q = 1$)

We repeat the analysis of the previous section, now introducing the self-weight contribution. This amounts to the full system of equations (13), where $q(x) = y(x)$, $I[x, y] = \langle y, 1 \rangle_{[x, 1]}$, and $I_y[x, y] = (1 - x)$. Thus, we can simplify $\gamma_0 = \lambda_Q y$, $\gamma_1 = \lambda_P + \lambda_Q \langle y, 1 \rangle_{[x, 1]}$, and $\gamma_2 = \lambda_Q(1 - x)$.

We remark that, due to the self-weight, buckling may also happen with $\lambda_P = 0$. This will be discussed in the next section, and we now fix $\lambda_Q = 1$. In the following, we will refer to the beam loaded only by the tip force as the “light beam”, whereas the “heavy beam” also accounts for the self-weight.

We refer to Figure 4 where, against the left axis, we plot $\Delta_{\Omega}^{(SW)} := \Omega/\Omega^{(SW)} - 1$, which is the relative difference between the reduced frequency for the light beam (Ω , same as in the previous section), and that of the heavy beam ($\Omega^{(SW)}$). For the uniform design, this quantity is clearly larger than one, as the self-weight introduces an additional compression, further reducing the vibration frequency. Also, it is monotonically increasing with λ_P for all the beam configurations, and this comes from the coupling of λ_Q in the v_x and v_{xx} terms of the state equation.

Let us focus the discussion on the CF configuration first. For the uniform beam (blue dashed curve), the self-weight alone slightly reduces the frequency ($\Delta_{\Omega}^{(SW)} \approx 0.125\%$ for $\lambda_P = 0$). Then, its effect increases with increasing λ_P , and for $\lambda_P \approx 1$ we have $\Delta_{\Omega}^{(SW)} \approx 38\%$. The trend is the opposite when looking at the relative difference in the frequency attained by the optimized beam (blue continuous curve). Now the largest difference happens for $\lambda_P = 0$ ($\Delta_{\Omega}^{(SW)} \approx 28\%$), as the self-weight is the first source of compression perturbing the optimal design from the one corresponding to the unloaded beam. Then, as λ_P increases and the size-independent compression dominates the self-weight, $\Delta_{\Omega}^{(SW)}$ quickly drops to a few $\%$. However, for the optimized frequency, the ratio $\Delta_{\Omega}^{(SW)}$ is non-monotonous and after reaching the minimum at $\lambda_P = l_4 = 0.385$, the influence of self-weight (slightly) increases again, giving $\Delta_{\Omega}^{(SW)} \approx 0.415\%$ for $\lambda_P \approx 1$.

This trend is also reflected by the relative difference between the frequency gains for the light and heavy beams, $\Delta_{r_{\Omega}}^{(SW)} := r_{\Omega}/r_{\Omega}^{(SW)} - 1$ (see red curves in Figure 4). For low magnitudes of the tip compression we have $\Delta_{r_{\Omega}}^{(SW)} > 0$, and the optimization gives a higher frequency gain for the light beam, compared to the heavy one. For $\lambda_P = l_5 \approx 0.455$ we have $\Delta_{r_{\Omega}}^{(SW)} = 0$, and the frequency gains for the heavy and light beams are exactly the same. Then, for higher values of the tip compression we have $\Delta_{r_{\Omega}}^{(SW)} < 0$ and, for $\lambda_P \approx 1$ the heavy beam benefits from the optimization about 27.5% more, compared to the light one. However, we observe that apart from the two regions where λ_P is close to zero or one, the self-weight has a very little influence on the optimization outcomes. For instance, when $0.175 \leq \lambda_P \leq 0.655$ we have $|\Delta_{r_{\Omega}}^{(SW)}| \leq 10^{-3}$, and therefore the self-weight has a negligible impact on the frequency gain (see horizontal lines in Figure 4).

The CS and CC configurations share the same qualitative behaviour of the CF, though we have different values for the ratios $\Delta_{\Omega}^{(SW)}$, $\Delta_{r_{\Omega}}^{(SW)}$, and location of points l_4 and l_5 (see also Table 1). Also, both configurations show a much wider range where $|\Delta_{r_{\Omega}}^{(SW)}| \leq 10^{-3}$, and therefore the self-weight has negligible influence on the optimization outcomes ($\lambda_P \in [0.01, 0.88]$ and $\lambda_P \in [0.01, 0.86]$ for the CS and CC beams, respectively). This can be clearly seen by the trend of the red curves in Figure 4, for the CF and CS beams. For the SS configuration, both $\Delta_{\Omega}^{(SW)}$ and $\Delta_{r_{\Omega}}^{(SW)}$

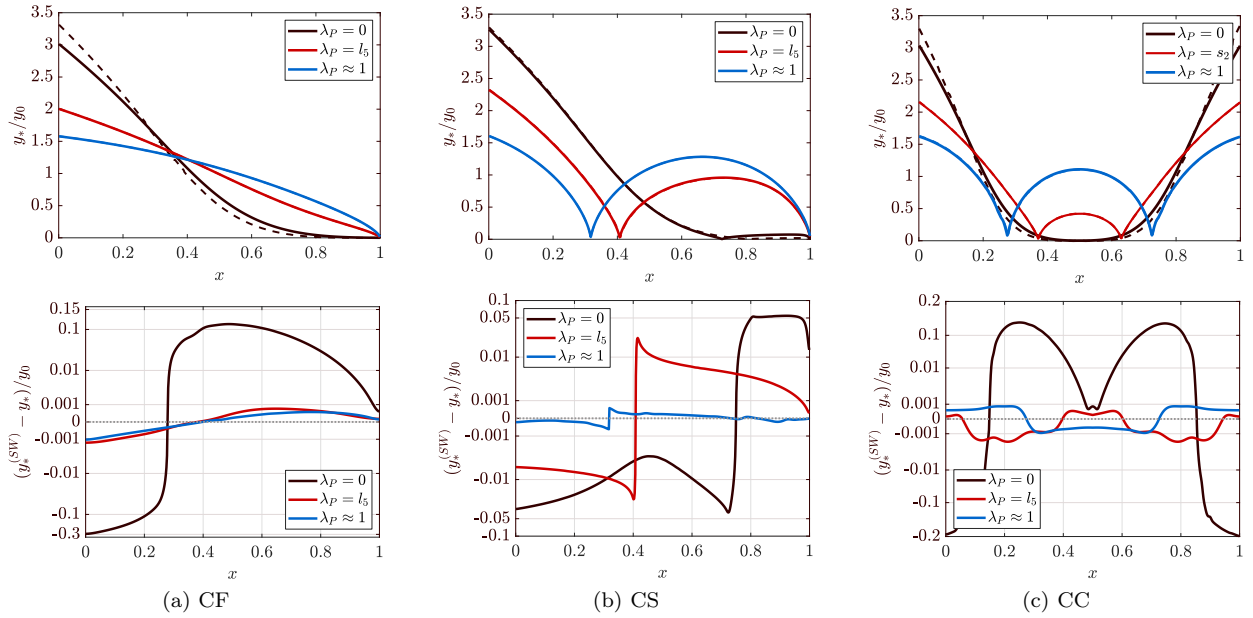


Figure 5: Comparison between the optimized size distribution for the heavy beam (continuous line) and for the light beam (dashed line), for three values of the tip design-independent compression λ_P . We remark that $\lambda_P = l_5$ correspond to the tip compression at which the self-weight has no influence on the frequency gain. The plots in the bottom row show the log-scaled relative difference between the two size distributions

are monotonically increasing and decreasing, respectively. Therefore, as λ_P increases, we gain systematically more when optimizing the heavy beam, compared to the light one.

The effect of self-weight on the optimized size distributions is shown in Figure 5. Here, the SS beam is not shown, as for this case we have only minor design changes. The plots in the top row compare the relative size distribution of the light (dashed line) and of the heavy beams (continuous line), for three notable tip compression values: $\lambda_P = 0$, $\lambda_P \approx 1$, and $\lambda_P = l_5$. For all the beam configurations, we can distinguish between $y_*^{(SW)}$ and y_* only for $\lambda_P = 0$, as the self-weight has the effect of reducing the size at the clamped ends, while increasing it at the points where the unloaded beam would develop a Type II singularity. For the compression levels $\lambda_P = l_5$ and $\lambda_P \approx 1$, $y_*^{(SW)}$ and y_* are almost indistinguishable; however, we can refer to the plots of the bottom row, showing a logarithmic plot of their difference, and recognize a similar trend. For $\lambda_P = 0$, the CF beam's sizes show the largest differences due to self-weight. At $x = 0$ the size is reduced of about 30%, whereas the maximum increase of about 13.5% occurs at $x \approx 0.5$. For the CS beam, the size's maximum decrease and increase are lower (4.3% and 5.5%), and both occur within the domain, at about $x \approx 0.75$. For the CC beam, the size is reduced of about 24% at the clamped ends, and the maximum increase (10%) occurs, interestingly, at the symmetrical locations $x \approx 0.25$ and $x \approx 0.75$, and not at the mid-point. In all cases, for the higher compression levels the size relative differences quickly drops to very small values. However, it is interesting to note that for the CS configuration we still have size differences up to $\pm 2\%$, corresponding to $\lambda_P = l_5$, without affecting the frequency gain.

Summarizing, the self-weight contribution sensibly impacts the frequency optimization both when considering zero or high values of the design-independent compression. In particular, frequency optimization becomes highly beneficial for heavy and highly compressed columns. Otherwise, the influence of self-weight on the optimization outcome is very small.

3.3. Influence of the distributed axial load alone ($\lambda_P = 0$, $q(x) = y(x)$, $\lambda_Q \geq 0$)

We now remove the size-independent compression, while keeping the distributed axial load proportional to self-weight; thus the coefficients in (13) become $\gamma_0 = \lambda_Q y$, $\gamma_1 = \lambda_Q \langle y, 1 \rangle_{[x,1]}$, and $\gamma_2 = \lambda_Q (1 - x)$.

We increase the axial load multiplier up to $\lambda_Q = 0.995$, with $\Delta\lambda_Q = 1/200$. Again, we have an inverse relationship between Ω_0^2 and λ_Q and, for the uniform design, the multiplier causing buckling under self-weight (and thus $\Omega_0 = 0$) is $\lambda_Q^{Cr} = \{942.97, 397.52, 2664.6, 3781.8\}$, for the SS, CF, CS and CC configurations, respectively [56].

We point out that scaling λ_Q , when considering self-weight, can still be given a meaning as a ‘‘tallest column’’ design problem[35, 16]. Indeed, from (4) we have $\lambda_Q \propto L^4$ and $\varpi/\lambda_Q \propto L$. Therefore, we may alternatively interpret this as the optimal design of a the tallest column with the same frequency and buckling strength of the initial one. However, the main difference with the classical tallest column problem is that now λ_Q is set as a parameter.

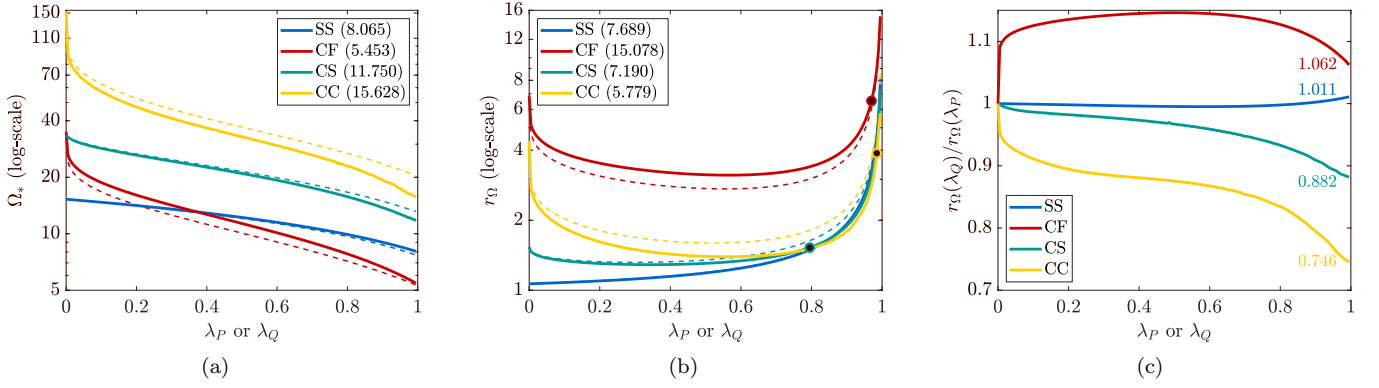


Figure 6: Optimized frequency (a), and the frequency gain (b) for each level of the axial load multiplier λ_Q and for the four beam configurations. The dashed curves correspond to the case of tip compression λ_P , and are the same as in Figure 2. The black dots in (b) mark the points $\lambda_Q = l_6$, where $r_\Omega(l_6) = r_\Omega(0)$, where the frequency gain matches that of the unloaded beam. (c) shows the ratio between the frequency gain factors for the cases of distributed axial load and tip compression

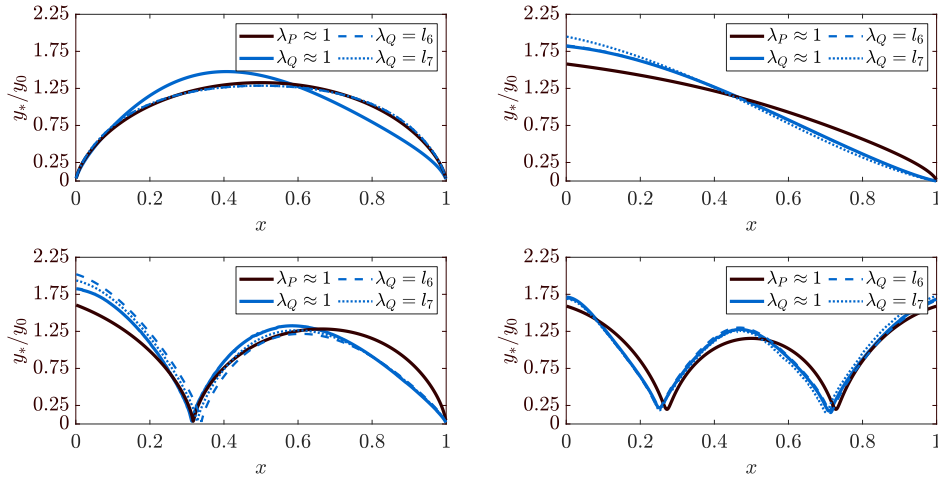


Figure 7: Comparison between the optimal size distribution for nearly critical compression, considering the tip force alone ($\lambda_P \approx 1$), or the distributed axial load proportional to self-weight alone ($\lambda_Q \approx 1$). The two designs shown as a dashed and dotted lines correspond to the compression level $\lambda_Q = l_6$, where $r_\Omega(l_6) = r_\Omega(0)$, and to $\lambda_Q = l_7$, respectively. This latter design has the same buckling strength of the uniform one (see Subsection 3.4)

Figure 6 (a,b) show the trend of the optimized frequency $\Omega_* = \Omega_*(\lambda_Q)$ and frequency gain $r_\Omega = r_\Omega(\lambda_Q)$, for the four beam configurations. For comparison, we also display, as dashed lines, the same curves corresponding to the case of tip compression, identical to those in Figure 2. For all the beam configurations, we highlight the points $\lambda_Q = l_6$, where $r_\Omega(l_6) = r_\Omega(0)$ (see also Table 1). As for the case of tip compression, we have $l_6 = 0$ for the SS beam, and the frequency gain is monotonically increasing with the load parameter.

For the SS and CF beams, the optimized frequency Ω_* corresponding to a given λ_Q is always larger than that obtained for the same value of λ_P ; also, we have $r_\Omega(\lambda_Q) > r_\Omega(\lambda_P)$. Therefore, for these two configurations frequency optimization leads to larger gains when the beam is loaded by its own self-weight, compared to the tip force compression. The opposite is true for the CS and CC beams, as we now have $\Omega_*(\lambda_Q) < \Omega_*(\lambda_P)$ and $r_\Omega(\lambda_Q) < r_\Omega(\lambda_P)$, for all values of the load multiplier.

These trends are clearly visible from Figure 6(c) showing the ratio $r_\Omega(\lambda_Q)/r_\Omega(\lambda_P)$, which is always above one for the SS and CF beams, and always below one for the CS and CC. For the SS configuration the ratio only shows a mild variation, whereas, for the CF beam we have a sudden increase, as the slightest amount of tip compression reduces Ω_* much more than the slightest amount of axial load. Then we reach the maximum ratio $r_\Omega(\lambda_Q)/r_\Omega(\lambda_P) \approx 1.15$ for $\lambda_Q = 0.495$, and a slight decrease after. For the CS and CC configurations the decrease of this ratio is monotonic, and very strong for the CC. For the case $\lambda_Q \approx 1$ we have frequency gains 1.1% and 6.2% larger, for the SS and CF configurations, and 22% and 36% smaller, for the CS and CC configurations, compared to the case $\lambda_P \approx 1$.

Figure 7 displays the comparison between the optimized size distribution corresponding to the axially distributed and tip load. The designs are compared for nearly critical compression values ($\lambda_Q \approx 1$ and $\lambda_P \approx 1$), where the two show the largest differences. We see that the optimal size distributions change from those in Figure 3, to a design

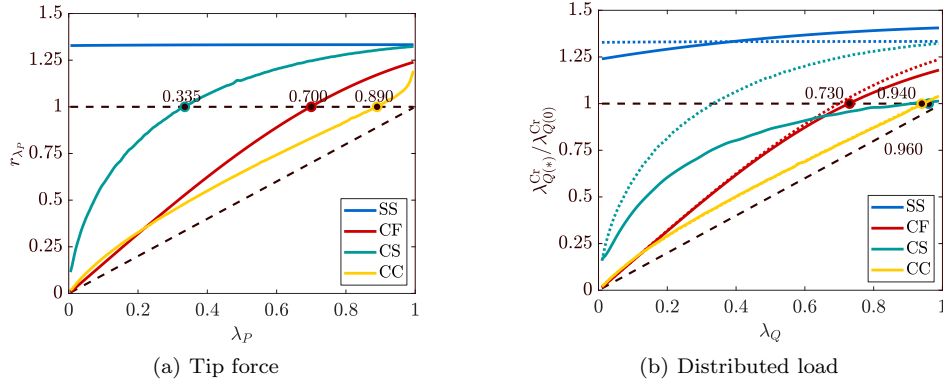


Figure 8: (a) Ratio between the critical load of the optimized and uniform beams, depending on the compression level considered in the optimization Equation (12). The ratios r_{λ_P} and r_{λ_Q} are always larger than the current critical load $(\lambda^{Cr})^{-1}$ (dashed line at 45°). The black dots mark the points where $r_{\lambda_P} = 1$, and the critical load of the optimized beam equals that of the initial one. The dashed lines in plot (b) report the curves in (a), for comparison

closer to the tallest column one [16], clearly showing a magnification of the self-weight effect. We also show the designs corresponding to the two notable compression level $\lambda_Q = l_6$, where the frequency gain matches the one for the unloaded beam, and $\lambda_Q = l_7$, where the critical load matches that of the initial design (see discussion in the next section).

We point out that, in none of these cases the design develops a Type II singularity and even for $\lambda_Q \approx 0$ we have $y_* = y_{\min}$ only at isolated points. This, which may look counter-intuitive, is due to the fact that the multiplier λ_Q is here a constant parameter, and is not optimized for as in the classical tallest column formulation[35, 16, 38].

3.4. Indirect effect on the buckling load factor

Finally we investigate the indirect effect of maximizing Ω_1 at a given compression level, on the beams' critical load. This latter, which is *not* directly optimized, may either increase or decrease during the optimization. Figure 8 shows the ratios $r_{\lambda_P} := \lambda_{P(*)}^{Cr} / \lambda_{P(0)}^{Cr}$ (viz. $r_{\lambda_Q} := \lambda_{Q(0)}^{Cr} / \lambda_{Q(*)}^{Cr}$), between the critical load of the optimized beam and that of the uniform one, depending on the magnitude of the tip compression λ_P , or axial distributed load λ_Q . The critical load multiplier of the compressed, uniform beam clearly follows the relationship $\lambda_{P(0)}^{Cr} = 1/\lambda_P$ (viz., $\lambda_{Q(0)}^{Cr} = 1/\lambda_Q$), plotted as a black dashed line in Figure 8. Since both r_{λ_P} and r_{λ_Q} are always above this line, our assumption of harmonic motion is valid.

For the SS beam, $r_{\lambda_P} > 1$ and $r_{\lambda_Q} > 1$ for all compression levels, so for this configuration the maximization of the vibration frequency always gives, as a side effect, the increase of the critical load. Also, the range of variation of the two ratios is very narrow for the SS beam, especially when considering the tip compression, for which $1.328 \leq r_{\lambda_P} \leq 1.333$. This is expected, as in this case the optimized beam size is only minimally modified (see Figure 3(a)). On the other hand, we observe a larger range of variation when considering the axially distributed load, for which $1.23 \leq r_{\lambda_Q} \leq 1.406$, and this is consistent with the more marked modification of the beam's profile in this case (see Figure 7(a)).

For the CF, CS, and CC configurations the buckling capacity of the optimized design heavily depends on the compression level considered in the optimization. Up to the values $\lambda_P = l_3$ and $\lambda_Q = l_6$, respectively, we have $r_{\lambda_P} < 1$ and $r_{\lambda_Q} < 1$; therefore the optimized beam will show a lower buckling capacity than the uniform one. Then, for higher compression levels, the optimization also improves the beam's critical load. The designs corresponding to points l_3 and l_6 , featuring the same critical load as the uniform beam, are marked by green dotted lines in Figure 3 and Figure 7, respectively.

The first configuration to meet the condition $r_{\lambda_P} = 1$, at $l_3 = 0.335$, is the CS, whereas the last is the CC, at $l_3 = 0.89$. For the CF configuration, the value of r_{λ_P} is almost always between those of the CS and CC beams, and we have $l_3 = 0.7$. We also observe that r_{λ_P} has an approximately linear trend for the CF and CC configurations, whereas it shows a marked non-linear trend for the CS case. Moreover, for $\lambda_P \approx 1$ the CS beam attains a critical load which is slightly below (less than 1%) that of the SS beam, whereas the other two beam configurations attain lower values.

When considering the axially distributed load, we see some differences. First, for all beam configurations the same critical load of the uniform design is now reached for higher values of compression (thus $l_6 > l_3$). The trend of r_{λ_Q} for the CF and CC beams shows little deviations compared to the case of tip compression. On the contrary, the trend for the CS configuration is very different, and this configuration is now the last to reach $r_{\lambda_Q} = 1$, for a compression level close to the critical one ($l_6 = 0.96$).

	$\lambda_P = \lambda_Q = 0$	$\lambda_P \geq 0, \lambda_Q = 0$			$\lambda_P \geq 0, q(x) = y(x), \lambda_Q = 1$			$\lambda_P = 0, q(x) = y(x), \lambda_Q \geq 0$			
	r_Ω	$r_\Omega(\lambda_P \approx 1)$	$(l_1, r_\Omega(l_1))$	l_2	l_3	$r_\Omega^{(SW)}(\lambda_P \approx 1)$	l_4	l_5	$r_\Omega(\lambda_Q \approx 1)$	l_6	l_7
SS	1.066	7.605	(0, 1.066)	0	-	8.489	-	0	7.689	0	-
CF	6.810	14.196	(0.56, 2.729)	0.975	0.7	19.513	0.385	0.455	15.078	0.97	0.730
CS	1.556	8.178	(0.3, 1.132)	0.755	0.335	8.465	0.375	0.355	7.190	0.795	0.96
CC	4.316	8.680	(0.525, 1.597)	0.975	0.89	8.971	0.435	0.42	5.775	0.895	0.94

Table 1: Summary of the frequency gains and notable points obtained in the numerical examples. The top labels follow the same naming of Subsection 3.1-Subsection 3.4. $r_\Omega(\cdot)$ is the frequency gain, for a given level of compression. The notable compression values are l_1 : λ_P value that gives the minimum frequency gain, (l_2 and l_6): λ_P and λ_Q value that gives the same frequency gain as for the unloaded beam, l_4 minimum frequency gain when considering the self-weight contribution, l_5 , zero influence of the self-weight on the frequency gain, (l_3 and l_7) same buckling capacity as the initial beam

4. Conclusions

We have investigated the effect of axial compression on the optimal sizing of beams for maximum fundamental vibration frequency, considering both a tip force generating a constant, control-independent compression, and a distributed axial load proportional to self-weight, giving a control-dependent compression. Some notable numerical results discussed throughout Section 3 are summarized in Table 1.

Both sources of compression have an impact on the frequency gains attainable by the optimization and, for all beam configurations but the SS, also on the optimal size distribution. As soon as compression is introduced, the optimal design deviates from that obtained for the unloaded beam (pure vibrations), and is prevented from developing singularities anywhere in the beam domain. This determines a substantial reduction of the optimal frequency gain, compared to the case of an unloaded beam. However, when looking at high compression levels, frequency optimization becomes much more beneficial, compared to the unloaded case. When the compression is just below the critical one, the frequency gains relative to those for the unloaded beam range between 2 to 7.1 for the tip force, and between 11.34 to 7.2 times for the distributed load proportional to self-weight.

When paired to the design-independent compression, the self-weight has a very little contribution for most of the “intermediate” values of the first. However, it does have an influence when the compression is close to the critical value, where again, its account leads to higher frequency gains, especially for the cantilever and simply supported configuration.

Acknowledgements

The author gratefully acknowledges the support of the Villum Foundation, through the Villum Investigator project “InnoTop”.

Appendix A. Remarks on the local behaviour of the dynamic solution

Here we summarize the classical local asymptotic analysis for the optimal design of a purely vibrating beam, recalling the definition of the two types of singularities occurring in this case[21, 33, 40].

For the optimal design of an uncompressed beam ($\lambda_Q = \lambda_P = 0$), for maximum frequency of vibration, the system governing the optimality (13) reduces to

$$\begin{aligned}
(y^p v_{xx})_{xx} - \bar{\Omega}^2 y v &= 0 \\
p y^{p-1} v_{xx}^2 - \bar{\Omega}^2 v^2 - \bar{\Omega}^2 (p-1) &= 0 \\
B(y, v) &= 0 \\
[[M v_x]]_{x_k} &= 0, \quad k = 1, \dots, n_I \\
[[T v]]_{x_k} &= 0, \quad k = 1, \dots, n_{II}
\end{aligned} \tag{A.1}$$

where we have also introduced the boundary operator $B(y, v)$, and we allowed for a finite number of jumps in the optimal energy distribution associated with the bending moment $M := y^p v_{xx}$ and shear force $T := (y^p v_{xx})_x$. Continuity of these internal actions must hold everywhere within the beam domain, as we do not consider point loads[24], but depending on the vanishing of either or both of them, we can identify two types of points where the optimal size $y_* \rightarrow 0$, and some of the response components becomes singular.

The first set of points is defined as follows:

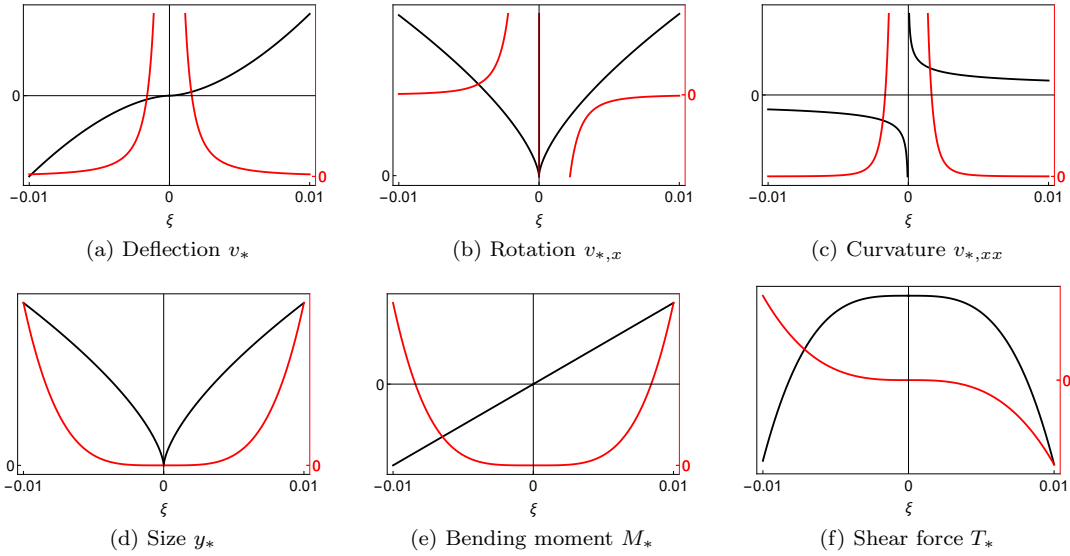


Figure A.9: Optimal response functions, size distribution, and internal actions near a Type I (black curves, plotted against the left axis), and Type II (red curves, plotted against the right axis) point, according to (A.4) and (A.6)

Definition (Type I singularity). Let $x_k^{(I)} \in [0, 1]$ be a point where $M_*(x_k^{(I)}) = 0$, and $T_*(x_k^{(I)}) \neq 0$. Then, $y_*(\xi) = O(\xi^{1/3})$, where $\xi = |x - x_k^{(I)}|$. Also, v_* is continuous, its derivative $v_{*,x}$ has a finite jump, and the curvature $v_{*,xx}$ is singular at $x_k^{(I)}$.

At such points, the continuity of the bending moment is automatically fulfilled, $M_*(x_k^{(I)}) = 0$, and therefore $v_{*,x}(x_k^{(I)})$ can have a finite jump, provided that $y_*(x_k^{(I)}) = 0$, such that the energy product $\llbracket y_*^p v_{*,xx}^2 \rrbracket_{x_k^{(I)}}$ remains finite. Mechanically, this point mimics the introduction of a hinge in the beam's domain.

The second set of points leading to a response singularity can be introduced as follows:

Definition (Type II singularity). Let $x_k^{(II)} \in [0, 1]$ be a point where $M_*(x_k^{(II)}) = T_*(x_k^{(II)}) = 0$. Then, $y_*(\xi) = O(\xi^2)$, where $\xi = |x - x_k^{(II)}|$. Also, v_* has a jump, and both $v_{*,x}$ and $v_{*,xx}$ are singular at $x_k^{(II)}$.

At such points both internal actions are vanishing, and this allows for a jump on v_* . Then, the singularity of $v_{*,x}(x_k^{(II)})$ and $v_{*,xx}(x_k^{(II)})$ requires $y_*(x_k^{(II)}) = 0$, in order to have finite energy products $\llbracket y_*^p v_{*,xx}^2 \rrbracket_{x_k^{(II)}}$ and $\llbracket (y_*^p v_{*,xx}^2)_x v \rrbracket_{x_k^{(II)}}$. Mechanically, this second singularity represents a complete separation of the beam.

The behaviour of the response functions near these two types of points can be deduced by an asymptotic analysis on the following non-linear differential equation

$$\left[\left(\frac{\bar{\Omega}^2 (v_x^2 + p - 1)}{p v_{xx}^2} \right)^{p(1-p)} v_{xx} \right]_{xx} - \left(\frac{\bar{\Omega}^2 (v^2 + p - 1)}{p v_{xx}^2} \right)^{1-p} v = 0 \quad (\text{A.2})$$

obtained by eliminating the expression for y_* from the state equation in (A.1). Then we represent the deflection $v_*(\xi)$ according to a regular, or a singular expansion [26].

In the first case we assume $v^{(I)}(\xi) = a_0 + a_1 \xi^r$, where $r \in \mathbb{Q}$ and $(a_0, a_1) \in \mathbb{R}$, and substituting within (A.2), we obtain the residual

$$\mathcal{R}[v^{(I)}] = \frac{\bar{\Omega}^2 \xi^{4-3r}}{t_0} [(a_0^4 + 3(1 + 2a_0^2))t_1 + o(\xi)] = 0 \quad (\text{A.3})$$

where $t_0 = 4a_2 r^3 (r-1)^3$ and $t_1 = 3(r-2)(3r-5)$. Non-trivial solutions to (A.3) require $t_1 = 0$, while $t_0 \neq 0$. This correspond to the pair of solutions $r_1 = 5/3$ and $r_2 = 2$, which plugged in (A.3) give

$$\lim_{\xi \rightarrow 0^+} \mathcal{R}\{r_1, r_2\} = \left\{ 0, \frac{(a_0 + a_0^3) \bar{\Omega}^2}{8a_2^2} \right\}$$

and therefore only the solution $r = 5/3$ is acceptable. The behaviour of the functions near a Type I points is (see Figure A.9)

$$\begin{aligned} v_*(\xi) &= a_0 + a_1 \xi + \xi^{5/3}, & v_{*,x}(\xi) &= a_1 + a_2 \xi^{2/3}, & v_{*,xx}(\xi) &= a_3 \xi^{-1/3} \\ y_*(\xi) &= a_4 \xi^{1/3} + O(\xi), & M_*(\xi) &= \xi + O(\xi^2), & T_*(\xi) &= a_5 + O(\xi) \end{aligned} \quad (\text{A.4})$$

where the expression of the a_i coefficients can be found in [40].

If we consider the singular expansion $v^{(\text{II})}(\xi) = b_0 \xi^{-s}$, $s \in \mathbb{N}_+$, $b_0 \in \mathbb{R}$ the residual of (A.2) becomes

$$\mathcal{R}[v^{(\text{II})}] = \frac{\bar{\Omega}^2 \xi^{4-s}}{q_0} [-b_1^4 q_1 + o(\xi^{2s})] = 0 \quad (\text{A.5})$$

where $q_0 = 4b_1^3 s^3 (s+1)^3$ and $q_1 = (s+15)(s-2)$. Now the only acceptable solution is $s = 2$, and the functions near a Type II point behave as follows (see Figure A.9)

$$\begin{aligned} v_*(\xi) &= b_0 \xi^{-2}, & v_{*,x}(\xi) &= -b_1 \xi^{-3}, & v_{*,xx}(\xi) &= b_2 \xi^{-4} \\ y_*(\xi) &= b_3 \xi^2, & M_*(\xi) &= b_4 \xi^4, & T_*(\xi) &= b_5 \xi^3 \end{aligned} \quad (\text{A.6})$$

where the expression of the b_i coefficients can be found in [40].

References

- [1] Adali, S.: Optimal shape and non-homogeneity of a non-uniformly compressed column. *International Journal of Solids and Structures* **15**(12), 935–949 (1979). DOI [https://doi.org/10.1016/0020-7683\(79\)90023-4](https://doi.org/10.1016/0020-7683(79)90023-4)
- [2] Atanackovic, T., Glavardanov, V.: Optimal shape of a heavy compressed column. *Structural and Multidisciplinary Optimization* **28**(6), 388–396 (2004). DOI [10.1007/s00158-004-0457-1](https://doi.org/10.1007/s00158-004-0457-1). URL <http://link.springer.com/10.1007/s00158-004-0457-1>
- [3] Atanackovic, T.M.: Optimal shape of column with own weight: bi and single modal optimization. *Meccanica* **41**, 173–196 (2006)
- [4] Atanackovic, T.M., Seyranian, A.P.: Application of Pontryagin’s principle to bimodal optimization problems. *Structural and Multidisciplinary Optimization* **37**(1), 1–12 (2008). DOI [10.1007/s00158-007-0211-6](https://doi.org/10.1007/s00158-007-0211-6). URL <http://link.springer.com/10.1007/s00158-007-0211-6>
- [5] Banichuk, N.V.: *Problems and Methods of Optimal Structural Design*. Springer US, Boston, MA (1983). DOI [10.1007/978-1-4613-3676-1](https://doi.org/10.1007/978-1-4613-3676-1). URL <http://link.springer.com/10.1007/978-1-4613-3676-1>
- [6] Barnes, D.C.: Extremal Problems for Eigenvalue Functionals. *SIAM Journal on Mathematical Analysis* **16**(6) (1985). DOI [10.1137/0516092](https://doi.org/10.1137/0516092)
- [7] Barnes, D.C.: Extremal Problems for Eigenvalue Functionals. II. *SIAM Journal on Mathematical Analysis* **19**(5), 1151–1161 (1988). DOI [10.1137/0519080](https://doi.org/10.1137/0519080). URL <http://epubs.siam.org/doi/10.1137/0519080>
- [8] Barnes, D.C.: The shape of the strongest column is arbitrarily close to the shape of the weakest column. *Quarterly of Applied Mathematics* **46**(4) (1988). DOI [10.1090/qam/973378](https://doi.org/10.1090/qam/973378)
- [9] Barnes, E.R.: Some min-max problems arising in optimal design studies. In: *Control Theory of Systems Governed by Partial Differential Equations*, pp. 177–208. Elsevier (1977). DOI [10.1016/B978-0-12-068640-7.50010-6](https://doi.org/10.1016/B978-0-12-068640-7.50010-6). URL <https://linkinghub.elsevier.com/retrieve/pii/B9780120686407500106>
- [10] Barnes, E.R.: The shape of the strongest column and some related extremal eigenvalue problems. *Quarterly of Applied Mathematics* **34**(4) (1977). DOI [10.1090/qam/493674](https://doi.org/10.1090/qam/493674)
- [11] Brach, R.: On the extremal fundamental frequencies of vibrating beams. *International Journal of Solids and Structures* **4**(7), 667–674 (1968). DOI [10.1016/0020-7683\(68\)90068-1](https://doi.org/10.1016/0020-7683(68)90068-1). URL <https://linkinghub.elsevier.com/retrieve/pii/0020768368900681>
- [12] Brach, R.M.: On optimal design of vibrating structures. *Journal of Optimization Theory and Applications* **11**(6), 662–667 (1973). DOI [10.1007/BF00935565](https://doi.org/10.1007/BF00935565). URL <http://link.springer.com/10.1007/BF00935565>
- [13] Bulson, P.: Optimal structural design under stability constraints. *Engineering Structures* **12**(1), 69–70 (1990). DOI [10.1016/0141-0296\(90\)90047-V](https://doi.org/10.1016/0141-0296(90)90047-V). URL <https://linkinghub.elsevier.com/retrieve/pii/014102969090047V>
- [14] Carmichael, D.: Singular optimal control problems in the design of vibrating structures. *Journal of Sound and Vibration* **53**(2) (1977). DOI [10.1016/0022-460X\(77\)90468-0](https://doi.org/10.1016/0022-460X(77)90468-0)
- [15] Charrett, D., Rozvany, G.: Extensions of the Prager-Shield theory of optimal plastic design. *International Journal of Non-Linear Mechanics* **7**(1), 51–64 (1972). DOI [10.1016/0020-7462\(72\)90021-2](https://doi.org/10.1016/0020-7462(72)90021-2). URL <https://linkinghub.elsevier.com/retrieve/pii/0020746272900212>

- [16] Cox, S.J., McCarthy, C.: The Shape of the Tallest Column. *SIAM Journal on Mathematical Analysis* **29**(3), 547–554 (1998). DOI 10.1137/S0036141097314537. URL <http://epubs.siam.org/doi/10.1137/S0036141097314537>
- [17] Egorov, Y.V.: On the Lagrange problem about the optimal form for circular hollow columns. *Comptes Rendus - Mecanique* **331**(10) (2003). DOI 10.1016/j.crme.2003.07.001
- [18] Egorov, Y.V.: On the tallest column. *Comptes Rendus. Mécanique* **338**(5), 266–270 (2010). DOI 10.1016/j.crme.2010.05.001
- [19] Gajewski, A., Piekarski, Z.: Optimal structural design of a vibrating beam with periodically varying cross-section. *Structural Optimization* **7**(1-2), 112–116 (1994). DOI 10.1007/BF01742515. URL <http://link.springer.com/10.1007/BF01742515>
- [20] Gierliński, J., Mróz, Z.: Optimal design of elastic plates and beams taking large deflections and shear forces into account. *Acta Mechanica* **39**(1-2) (1981). DOI 10.1007/BF01173194
- [21] Gjelsvik, A.: Minimum weight design of continuous beams. *International Journal of Solids and Structures* **7**(10) (1971). DOI 10.1016/0020-7683(71)90054-0
- [22] Haftka, R.T., Gürdal, Z.: Elements of Structural Optimization, *Solid Mechanics And Its Applications*, vol. 11. Springer Netherlands, Dordrecht (1992). DOI 10.1007/978-94-011-2550-5. URL <http://link.springer.com/10.1007/978-94-011-2550-5>
- [23] Hanaoka, M., Washizu, K.: Optimum design of Beck's column. *Computers & Structures* **11**(6), 473–480 (1980). DOI 10.1016/0045-7949(80)90054-1. URL <https://linkinghub.elsevier.com/retrieve/pii/0045794980900541>
- [24] Hartmann, F.: The Mathematical Foundation of Structural Mechanics. Springer Berlin Heidelberg, Berlin, Heidelberg (1985). DOI 10.1007/978-3-642-82401-2. URL <http://link.springer.com/10.1007/978-3-642-82401-2>
- [25] Haug, E.J., Rousselet, B.: Design Sensitivity Analysis in Structural Mechanics. I. Static Response Variations. *Journal of Structural Mechanics* **8**(1), 17–41 (1980). DOI 10.1080/03601218008907351. URL <http://www.tandfonline.com/doi/abs/10.1080/03601218008907351>
- [26] Hinch, E.J.: Perturbation Methods. Cambridge Texts in Applied Mathematics. Cambridge University Press (1991)
- [27] Holmáker, K.: Some Mathematical Aspects on a Problem of the Optimal Design of a Vibrating Beam. *SIAM Journal on Mathematical Analysis* **18**(5), 1367–1377 (1987). DOI 10.1137/0518098. URL <http://epubs.siam.org/doi/10.1137/0518098>
- [28] Huang, N.C.: Optimal design of elastic structures for maximum stiffness. *International Journal of Solids and Structures* **4**(7), 689–700 (1968). DOI [https://doi.org/10.1016/0020-7683\(68\)90070-X](https://doi.org/10.1016/0020-7683(68)90070-X). URL <http://www.sciencedirect.com/science/article/pii/002076836890070X>
- [29] Huang, N.C.: Effect of shear deformation on optimal design of elastic beams. *International Journal of Solids and Structures* **7**(4) (1971). DOI 10.1016/0020-7683(71)90106-5
- [30] Huang, N.C.: Optimal Design of Elastic Beams for Minimum-Maximum Deflection. *Journal of Applied Mechanics* **38**(4), 1078–1081 (1971). DOI 10.1115/1.3408925. URL <https://asmedigitalcollection.asme.org/appliedmechanics/article/38/4/1078/423506/Optimal-Design-of-Elastic-Beams-f>
- [31] Hughes, T.J.R.: The Finite Element Method: Linear Static and Dynamic Finite Element Analysis. Prentice-Hall (1987)
- [32] Kamat, M.P.: Effect of shear deformations and rotary inertia on optimum beam frequencies. *International Journal for Numerical Methods in Engineering* **9**(1), 51–62 (1975). DOI 10.1002/nme.1620090105. URL <https://onlinelibrary.wiley.com/doi/10.1002/nme.1620090105>
- [33] Karihaloo, B.L., Niordson, F.I.: Optimum design of vibrating cantilevers. *Journal of Optimization Theory and Applications* **11**(6), 638–654 (1973). DOI 10.1007/BF00935563. URL <http://link.springer.com/10.1007/BF00935563>
- [34] Keller, J.B.: The shape of the strongest column. *Archive for Rational Mechanics and Analysis* **5**(1), 275–285 (1960). DOI 10.1007/BF00252909. URL <http://link.springer.com/10.1007/BF00252909>
- [35] Keller, J.B., Niordson, F.I.: The tallest column. *Jour. Math. Mech.* **16**(5), 433–446 (1966)
- [36] Keng-tung, C., Hua, D.: On dynamic optimization of Timoshenko beam. *Applied Mathematics and Mechanics* **4**(1), 69–77 (1983). DOI 10.1007/BF01896714. URL <http://link.springer.com/10.1007/BF01896714>
- [37] Krein, M.G.: On certain problems on the maximum and minimum of characteristic values and on the Lyapunov zones of stability (1955)

- [38] Maeve McCarthy, C.: The tallest column — optimality revisited. *Journal of Computational and Applied Mathematics* **101**(1-2), 27–37 (1999). DOI 10.1016/S0377-0427(98)00188-5. URL <https://linkinghub.elsevier.com/retrieve/pii/S0377042798001885>
- [39] Niordson, F.I.: On the optimal design of a vibrating beam. *Quarterly of Applied Mathematics* **23**(1), 47–53 (1965). DOI 10.1090/qam/175392. URL <https://www.ams.org/qam/1965-23-01/S0033-569X-1965-0175392-8/>
- [40] Olhoff, N.: Optimization of Vibrating Beams with Respect to Higher Order Natural Frequencies. *Journal of Structural Mechanics* **4**(1), 87–122 (1976). DOI 10.1080/03601217608907283. URL <http://www.tandfonline.com/doi/abs/10.1080/03601217608907283>
- [41] Olhoff, N., Niordson, F.I.: Some problems concerning singularities of optimal beams and columns. *Zeitschrift fuer angewandte Mathematik und Mechanik* **59** (1979)
- [42] Olhoff, N., Rasmussen, S.H.: On single and bimodal optimum buckling loads of clamped columns. *International Journal of Solids and Structures* **13**(7), 605–614 (1977). DOI 10.1016/0020-7683(77)90043-9. URL <https://linkinghub.elsevier.com/retrieve/pii/0020768377900439>
- [43] Payne, L.E.: Isoperimetric Inequalities for Eigenvalues and Their Applications. In: *Autovalori e autosoluzioni*, pp. 107–167. Springer Berlin Heidelberg, Berlin, Heidelberg (2011). DOI 10.1007/978-3-642-10994-2_{-}3. URL http://link.springer.com/10.1007/978-3-642-10994-2_3
- [44] Pedersen, P., Pedersen, N.L.: Analytical optimal designs for long and short statically determinate beam structures. *Structural and Multidisciplinary Optimization* **39**(4), 343–357 (2009). DOI 10.1007/s00158-008-0339-z. URL <http://link.springer.com/10.1007/s00158-008-0339-z>
- [45] Plaut, R.H., Virgin, L.N.: Optimal desing of cantilevered elastica for minimum tip deflection under self-weight. *SMO* **43**, 657–664 (2011)
- [46] Prager, W., Taylor, J.E.: Problems of Optimal Structural Design. *Journal of Applied Mechanics* **35**(1), 102–106 (1968). DOI 10.1115/1.3601120. URL <https://asmedigitalcollection.asme.org/appliedmechanics/article/35/1/102/387171/Problems-of-Optimal-Structural-Desi>
- [47] Rammerstorfer, F.: On the optimal distribution of the Young’s modulus of a vibrating, prestressed beam. *Journal of Sound and Vibration* **37**(1), 140–145 (1974). DOI 10.1016/S0022-460X(74)80064-7. URL <https://linkinghub.elsevier.com/retrieve/pii/S0022460X74800647>
- [48] Ringertz, U.T.: On the design of Beck’s column. *Structural Optimization* **8**(2-3), 120–124 (1994). DOI 10.1007/BF01743307. URL <http://link.springer.com/10.1007/BF01743307>
- [49] Rozvany, G., Yep, K., Ong, T., Karihaloo, B.: Optimal design of elastic beams under multiple design constraints. *International Journal of Solids and Structures* **24**(4), 331–349 (1988). DOI 10.1016/0020-7683(88)90065-0. URL <https://linkinghub.elsevier.com/retrieve/pii/0020768388900650>
- [50] Rozvany, G.I.N.: Optimal Plastic Design of Beams with Unspecified Actions or Reactions. pp. 115–159 (1989). DOI 10.1007/978-94-009-1161-1_{-}4. URL http://link.springer.com/10.1007/978-94-009-1161-1_4
- [51] Rozvany, G.I.N.: *Structural Design via Optimality Criteria*, vol. 8. Springer Netherlands, Dordrecht (1989). DOI 10.1007/978-94-009-1161-1
- [52] Sadiku, S.: Buckling load optimization for heavy elastic columns: a perturbation approach. *Structural and Multidisciplinary Optimization* **35**(5), 447–452 (2008). DOI 10.1007/s00158-007-0144-0. URL <http://link.springer.com/10.1007/s00158-007-0144-0>
- [53] Sadiku, S.: On the Application of the Perturbation Method in the Buckling Optimization of a Heavy Elastic Column of Constant Aspect Ratio. *Journal of Optimization Theory and Applications* **146**(1), 181–188 (2010). DOI 10.1007/s10957-010-9663-8. URL <http://link.springer.com/10.1007/s10957-010-9663-8>
- [54] Seyranian, A., Privalova, O.: The Lagrange problem on an optimal column: old and new results. *Structural and Multidisciplinary Optimization* **25**(5-6), 393–410 (2003). DOI 10.1007/s00158-003-0333-4. URL <http://link.springer.com/10.1007/s00158-003-0333-4>
- [55] Tadjbakhsh, I., Keller, J.B.: Strongest Columns and Isoperimetric Inequalities for Eigenvalues. *Journal of Applied Mechanics* **29**(1), 159–164 (1962). DOI 10.1115/1.3636448. URL <https://asmedigitalcollection.asme.org/appliedmechanics/article/29/1/159/424846/Strongest-Columns-and-Isoperimetric>
- [56] Timoshenko, S.P., Goodier, J.N.: *Theory of Elasticity*, third edn. McGraw Hill International Editions (1970)

- [57] Vepa, K.: On the existence of solutions to optimization problems with eigenvalue constraints. *Quarterly of Applied Mathematics* **31**(3) (1973). DOI 10.1090/qam/428893
- [58] Virgin, L.N.: *Vibration of axially loaded structures*. Cambridge University Press (2007)
- [59] Washizu, K.: *Variational Methods in Elasticity and Plasticity*, second edn. 01. Pergamon Press (1975)